JACS
JOURNAL OF THE AMERICAN CHEMICAL SOCIETY
Article
pubs.acs.org/JACS

p-Si/W_2C and p-Si/W_2C/Pt Photocathodes for the Hydrogen Evolution Reaction

Sean P. Berglund,[†] Huichao He,[†,∥] William D. Chemelewski,[†] Hugo Celio,[§] Andrei Dolocan,[§] and C. Buddie Mullins*[,†,‡]

[†]Department of Chemical Engineering, [‡]Department of Chemistry and Biochemistry, Center for Electrochemistry, [§]Texas Materials Institute, and Center for Nano- and Molecular Science, University of Texas at Austin, 1 University Station C0400, Austin, Texas 78712-0231, United States

[∥]College of Chemistry and Chemical Engineering, Chongqing University, Chongqing 400030, China

Supporting Information

ABSTRACT: p-Si/W_2C photocathodes are synthesized by evaporating tungsten metal in an ambient of ethylene gas to form tungsten semicarbide (W_2C) thin films on top of p-type silicon (p-Si) substrates. As deposited the thin films contain crystalline W_2C with a bulk W:C atomic ratio of approximately 2:1. The W_2C films demonstrate catalytic activity for the hydrogen evolution reaction (HER), and p-Si/W_2C photocathodes produce cathodic photocurrent at potentials more positive than 0.0 V vs RHE while bare p-Si photocathodes do not. The W_2C films are an effective support for Pt nanoparticles allowing for a considerable reduction in Pt loading. p-Si/W_2C/Pt photocathodes with Pt nanoparticles achieve photocurrent onset potentials and limiting photocurrent densities that are comparable to p-Si/Pt photocathodes with Pt loading nine times higher. This makes W_2C an earth abundant alternative to pure Pt for use as an electrocatalyst on photocathodes for the HER.

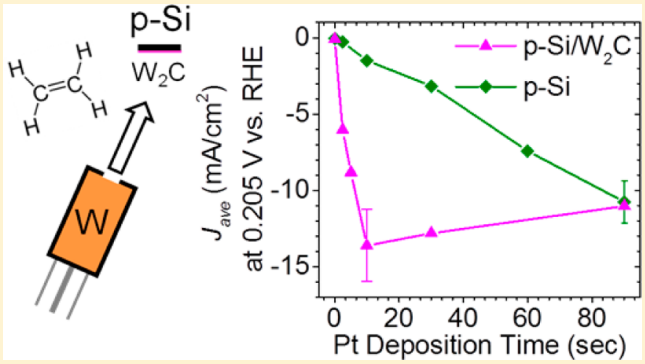

INTRODUCTION

Photoelectrochemical (PEC) water splitting is a potential processing route for hydrogen production using water and solar energy.[1,2] The hydrogen that is produced can be captured and utilized as a clean burning fuel or chemical feedstock. Practical implementation of PEC water splitting requires the development of PEC materials that are efficient, stable, and earth abundant. Two main types of materials are used for PEC water splitting. n-Type semiconductors are used as photoanodes for the oxygen evolution reaction (OER) and p-type semiconductors are used as photocathodes for the hydrogen evolution reaction (HER). One well-known p-type semiconductor material, p-type silicon (p-Si), can produce relatively high photocurrent densities for the HER, but it requires the addition of an electrocatalyst such as Pt to produce photocurrent at potentials more positive than 0 V vs RHE.[3−5] Unfortunately, Pt is an extremely scarce resource, making it expensive to use on a large scale for hydrogen production technologies.[6]

A more earth abundant alternative to Pt is tungsten carbide, which has shown similar electronic and catalytic properties to Pt for certain chemical reactions.[7,8] Both tungsten carbide (WC) and tungsten semicarbide (W_2C) have demonstrated relatively high activity as electrocatalysts for the HER along with good stability in neutral and acid solutions, although the exchange current densities (j_0) reported for tungsten carbide for the HER are lower than the values for Pt so tungsten carbide may not be sufficient to replace Pt entirely.[9−13] Nevertheless, tungsten carbide can be used as a support for Pt allowing for a reduction in Pt loading while retaining or improving activity for the HER.[14−17] For this reason, Pt-loaded tungsten carbide may be a useful electrocatalyst for p-type semiconductor photocathodes. Recently, tungsten carbide was tested as a cocatalyst on particulate photocatalysts such as p-type CdS and n-type Na-doped $SrTiO_3$.[18,19] We are unaware of any published results for WC or W_2C as electrocatalysts on p-type photocathodes for the HER. In this work we present the PEC results for p-Si photocathodes with a thin film of tungsten semicarbide (W_2C) deposited on the surface. In addition we show that W_2C is an effective support for Pt nanoparticles on p-Si photocathodes and can be used to reduce Pt loading by a factor of 9 while improving the PEC activity for the HER.

EXPERIMENTAL SECTION

Photocathode Synthesis. Photocathodes were prepared using p-type Si(111) substrates from two different suppliers (Addison Engineering, 540 μm thick, single-side polish, B doped, 0.1−10 ohm cm; EL-Cat Inc., 525 μm thick, double-side polish, B doped, 0.2−1.0 ohm cm). W_2C was deposited onto the polished side of the p-Si

Received: November 13, 2013
Published: January 6, 2014

   dx.doi.org/10.1021/ja411604k | J. Am. Chem. Soc. 2014, 136, 1535−1544

substrates using a technique known as reactive ballistic deposition (RBD), in which metal is evaporated onto a substrate inside a high vacuum chamber containing a reactant gas ambient.[20−24] For W_2C synthesis the evaporant source was a 0.125 in. diameter tungsten rod (Alfa Aesar, 99.95%) and the reactant gas was ethylene. The high vacuum chamber used for this study has been described previously.[25] Prior to deposition, the p-Si substrates were cleaned according to the following procedure. First they were rinsed and sonicated in reagent alcohol (PHARMCO-AAPER, 99.5%) for 15 min. Next they were rinsed with deionized water (DIW, <18 MΩ cm) and submerged in a freshly prepared solution of DIW:hydrogen peroxide (Fisher, 30%)/sulfuric acid (Fisher, ACS, 95.0 to 98.0 w/w %) = 1:2:6 for 15 min. Then they were rinsed with DIW and etched in a solution of 5 w/w % hydrofluoric acid (Sigma-Aldrich, ACS) for 5 min. Finally, they were rinsed with DIW, dried, and quickly loaded into the high vacuum chamber for deposition. The vacuum chamber was pumped down to a pressure of 5×10^{-8} Torr or lower. Deposition was done at ambient temperature using a W deposition rate of approximately 1.25 ML/min and a background ethylene pressure of 1×10^{-6} Torr resulting in an ethylene flux that was about 48 times higher than that of W. This was done to ensure an excess amount of carbon for the carburization reaction; however, X-ray diffraction and X-ray photoemission spectroscopy measurements revealed that these conditions resulted in the formation of W_2C rather than WC. Various thicknesses of W_2C were deposited onto the p-Si substrates. W_2C was also deposited onto fluorine doped tin oxide (FTO) coated glass substrates using the same conditions. The resulting photocathodes and electrodes are referred to as p-Si/W_2C and FTO/W_2C. After deposition some of the p-Si/W_2C photocathodes and FTO/W_2C electrodes were annealed in a tube furnace (MTI, OTF-1200X) as follows. The tube furnace was pumped to a pressure of 500 mTorr and then filled with Ar (Matheson Tri-Gas, 99.995%) to a pressure of 760 Torr. Next Ar was allowed to continuously purge the tube at 100 SCCM while the tube was heated with a temperature ramp rate of 10 °C/min and held at the desired temperature (350, 450, 550, 650 °C) for 2 h. For comparison purposes, Ni−Mo films were deposited onto p-Si substrates by coevaporation of nickel and molybdenum in the high vacuum chamber at pressures less than 5×10^{-8} Torr. The evaporant sources were a 0.25 in. diameter nickel rod (Alfa Aesar, 99.95%) and a 0.125 in. diameter molybdenum rod (Alfa Aesar, 99.95%).

Pt nanoparticles were deposited onto some of the p-Si and p-Si/W_2C photocathodes to make p-Si/Pt and p-Si/W_2C/Pt photocathodes using a current controlled pulsed deposition technique in a solution of 1 g/L $H_2PtCl_6{\cdot}6H_2O$ (Alfa Aesar, 99.95%).[26] During deposition the photocathodes were illuminated. The pulse sequence was 5 mA/cm^2 cathodic current for 10 ms followed by 5 mA/cm^2 anodic current for 2 ms followed by zero current for 100 ms, which was repeated for the desired deposition time. An example of the current controlled pulsed deposition sequence is included in the Supporting Information (Figure S1). Pt nanoparticles were deposited onto FTO/W_2C to make FTO/W_2C/Pt electrodes using the same technique but without illumination. Dense Pt films were synthesized by drop-casting 225 μL of 1 g/L $H_2PtCl_6{\cdot}6H_2O$ onto 1.5 cm × 1.5 cm FTO substrates, which were then annealed in the tube furnace at 350 °C for 2 h under 100 SCCM flow of 5% H_2/95% Ar.

Photocathode Characterization. When not in use, the p-Si/W_2C photocathodes were stored under vacuum (<1×10^{-7} Torr) to avoid unwanted oxidation. Bare p-Si photocathodes were cleaned, etched with 5 w/w % hydrofluoric acid, and rinsed with DIW immediately before PEC measurements using the procedure described above. The backside of each photocathode was scratched, painted with gallium indium eutectic (Alfa Aesar, 99.99%), and adhered to a piece of copper foil to create an ohmic contact. PEC measurements were performed using a three-electrode photoelectrochemical cell with a main compartment and two branched compartments separated by fritted disks (Ace Glass, 10−20 μm porosity). The cell was controlled using an electrochemical analyzer/workstation (CH Instruments CH660D). The working electrode (WE) was connected to the p-Si/W_2C photocathode or FTO/W_2C film, which was pressed onto the main compartment of the cell with an O-ring having an active area of 0.22 cm^2. The counter electrode (CE) was a 1 mm diameter Pt wire (Alfa Aesar, 99.95%) and the reference electrode (REF) was saturated Ag/AgCl (CH Instruments, CH111). The CE and REF were placed in the branched compartments of the cell. The cell was filled with 1 N sulfuric acid (Fisher, Certified 0.995−1.005 N, pH 0.3) that was continuously bubbled with nitrogen gas starting at least 30 min prior to measurements. The light source was a full spectrum solar simulator (Newport, model 9600, 150 W xenon lamp) with an AM 1.5 global filter (Newport). A thermopile sensor (Newport, model 818P-020-12) was used to set the illumination power density to 100 mW/cm^2. Potentials were converted to the reversible hydrogen electrode (RHE) scale. For 1 N sulfuric acid, RHE was measured at −0.205 V vs Ag/AgCl (see Figure S2 in the Supporting Information).

The material properties of the photocathodes were characterized using a variety of analytical instruments. X-ray diffraction (XRD) spectra were obtained using a Spider R-Axis diffractometer with an incident angle of 6 deg, a rotation speed of 6 deg/s, and Cu Kα radiation at 40 kV and 40 mA. UV−vis transmission and UV−vis transmission-reflectance measurements were taken on a Cary 5000 spectrophotometer and a Cary 500 spectrophotometer with an integrating sphere (Labsphere), respectively. A Zeiss Supra 40 VP scanning electron microscope (SEM) was used to capture SEM images. X-ray photoelectron spectroscopy (XPS) measurements were performed on a Kratos AXIS Ultra DLD spectrometer with Mg Kα radiation. Time-of-flight secondary ion mass spectrometer (TOF-SIMS) information was acquired using a TOF.SIMS 5 (ION-TOF GMBH). Atomic force microscopy (AFM) was performed on an Asylum Research MFP3D.

RESULTS

Photoelectrochemical Results. Figure 1 shows a linear sweep voltammetry (LSV) scan for p-Si and p-Si/W_2C photocathodes with and without Pt nanoparticles deposited on the surface in the dark and under white light illumination. The p-Si/W_2C photocathode had a W_2C film thickness of approximately 49 Å as determined by QCM measurements during deposition and cross-sectional SEM images. Before PEC

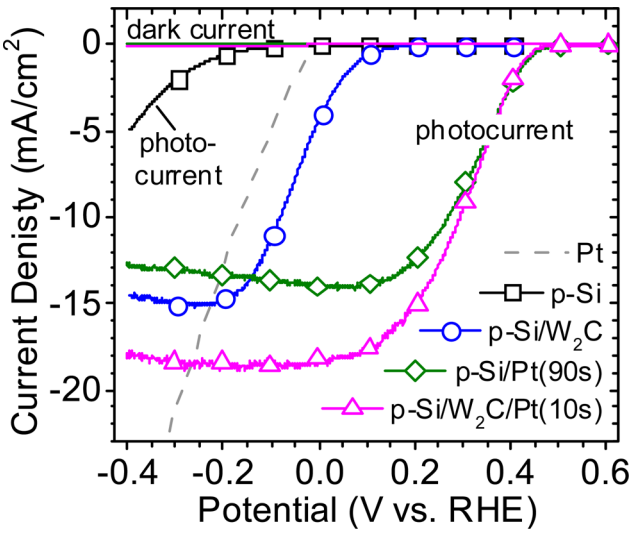

Figure 1. LSV scans (dark and white light) for p-Si and p-Si/W_2C photocathodes with and without Pt nanoparticles deposited on the surface. Current controlled pulsed deposition was used to deposit the Pt nanoparticles (total deposition times shown in parentheses). Before PEC measurements and Pt nanoparticle deposition, the p-Si/W_2C photocathode was annealed in Ar at 450 °C. The LSV scan for a dense Pt film on FTO is included. Measurements were conducted in N_2 purged 1 N H_2SO_4 using a scan rate of 25 mV/s and white light intensity of 100 mW/cm^2.

dx.doi.org/10.1021/ja411604k | J. Am. Chem. Soc. 2014, 136, 1535−1544

testing, the p-Si/W_2C photocathode was annealed under Ar flow at 450 °C for 2 h to improve the stability. The p-Si/Pt(90s) and p-Si/W_2C/Pt(10s) photocathodes had Pt nanoparticles deposited by current controlled pulsed deposition with total deposition times of 90 and 10 s, respectively. These deposition times resulted in the most positive photocurrent onset potentials and highest limiting photocurrent densities for p-Si and p-Si/W_2C. Also included in Figure 1, is the LSV scan for a dense Pt film on FTO. The LSV scans confirm that bare p-Si by itself is a poor photocathode for the HER since it did not show noticeable photocurrent until potentials more negative than 0.0 V vs RHE, and the photocurrent density was always lower than the current density for the dense Pt film. The LSV scans demonstrate that W_2C is an effective electrocatalyst for p-Si since the p-Si/W_2C photocathode had a photocurrent onset potential near 0.2 V vs RHE and it remained higher than the current density of the dense Pt film until −0.21 V vs RHE. As previously mentioned, Pt is more active than tungsten carbide for the HER. The addition of Pt nanoparticles to the p-Si and p-Si/W_2C photocathodes improved the photocurrent onset potentials to about 0.5 V vs RHE. The p-Si/W_2C/Pt(10s) photocathode showed a slightly higher limiting photocurrent of 18.6 mA/cm^2 compared that of p-Si/Pt(90s) at 14.0 mA/cm^2.

The optimal Pt deposition times of 90 and 10 s for p-Si and p-Si/W_2C were determined by varying the Pt deposition time and measuring the PEC activity. Figure 2 shows the average

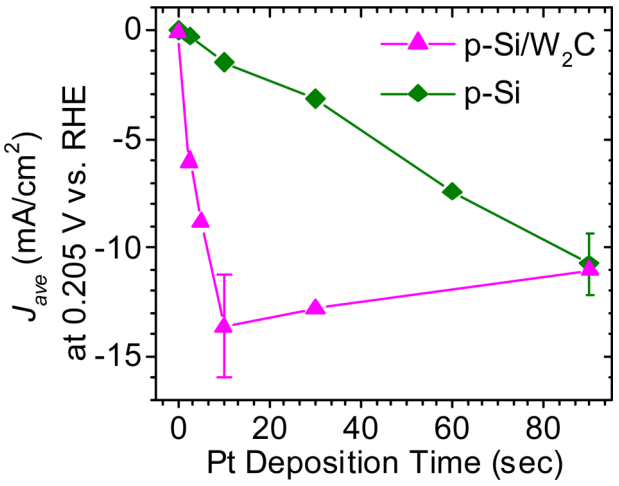

Figure 2. Average photocurrent density (J_{ave}) at 0.205 V vs RHE for p-Si and p-Si/W_2C photocathodes for various Pt current controlled pulsed deposition times. Before PEC measurements and Pt deposition the p-Si/W_2C photocathodes were annealed in Ar at 450 °C. The photocurrent density values were obtained from LSV scans under white light illumination in N_2 purged 1 N H_2SO_4 using a scan rate of 25 mV/s and white light intensity of 100 mW/cm^2. The error bars signify 1 standard deviation.

photocurrent density at 0.205 V vs RHE for p-Si and p-Si/W_2C photocathodes following different Pt deposition times. The p-Si/W_2C photocathodes reached the maximum photocurrent density after 10 s of Pt deposition compared to 90 s for p-Si. Since the pulsed deposition sequence is current controlled, the p-Si/W_2C photocathodes reach the maximum values after passing 1/9 as much charge as the p-Si photocathodes, and perhaps after depositing 1/9 as much Pt.

To qualitatively compare the amount of Pt deposited on the p-Si/Pt(90s) and p-Si/W_2C/Pt(10s) photocathodes we imaged them by SEM. Figure 3a shows that the p-Si/Pt(90s)

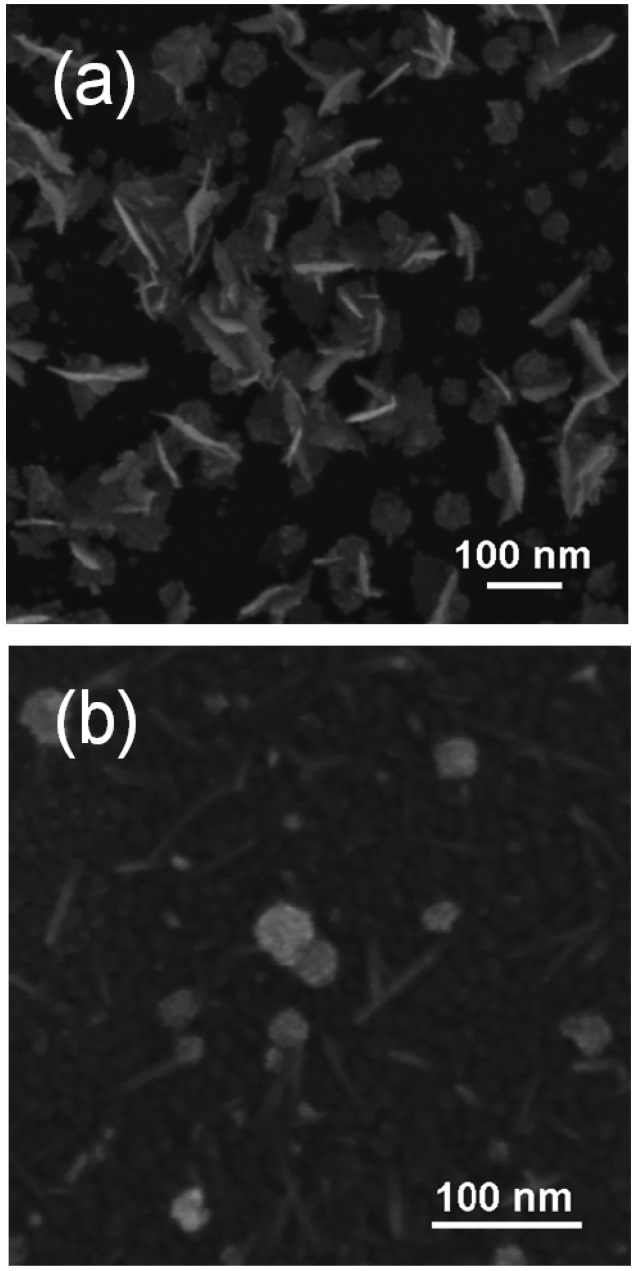

Figure 3. SEM images of (a) p-Si/Pt(90s) and (b) p-Si/W_2C/Pt(10s) photocathodes.

photocathodes were covered with Pt flakes on the order of 100 nm along with Pt nanoparticles that were 10−50 nm in diameter. The p-Si/W_2C/Pt(10s) photocathodes (Figure 3b) consisted of a rough layer of W_2C with scattered nanowires that were about 100 nm in length and a sparse coverage of Pt particles that were less than 50 nm in diameter. Clearly there was less Pt on the p-Si/W_2C/Pt(10s) photocathodes compared to p-Si/Pt(90s). Collectively, the PEC results and SEM images demonstrate that depositing a thin film of W_2C onto p-Si is an effective means of reducing the required Pt loading while retaining PEC activity for the HER.

dx.doi.org/10.1021/ja411604k | J. Am. Chem. Soc. 2014, 136, 1535−1544

The effect of Pt overlayers (Pt_{ML}) on top of WC(0001) and W_2C(0001) surfaces has been studied from a theoretical perspective via density functional theory (DFT) calculations.[17,27,28] Esposito et al. calculated that Pt_{ML}/WC(0001) and Pt_{ML}/W_2C(0001) possess hydrogen binding energies (HBEs) of −0.43 and −0.24 eV, which are close to the value of −0.46 eV for Pt(111).[17] Ma et al. concluded that for certain reaction sites the activation energy for hydrogen dissociation was similar for Pt_{ML}/WC(0001) and Pt(111) at 5.28 and 4.93 kJ/mol, respectively.[27] In addition, a strong intermetallic interaction between the Pt and WC(0001) was calculated involving the interfacial W and Pt d-states.[27,28] The HER activity of Pt_{ML}/WC(0001) was found to match the activity of Pt(111) rather than exceed it and no synergistic effect between Pt and WC(0001) was identified, but the possibility of hydrogen spillover was mentioned.[28] Hydrogen spillover has been validated for a variety of catalytic reactions on supports containing defective insulators, graphitic carbon, or reducible metal oxides such as WO_3, but spillover to a defect-free support such as SiO_2 has been calculated to be energetically unfavorable.[29−31] This implies that hydrogen spillover would not occur on the crystalline p-Si/Pt(90s) photocathodes. Though a recent study demonstrated hydrogen spillover from Pt metal to high quality silicon oxide for p-Si based metal insulator semiconductor (MIS) photocathodes.[32] The high activity of the Si/W_2C/Pt(10s) photocathodes with reduced Pt loading is likely the result of a strong Pt and W_2C intermetallic interaction combined with a reaction mechanism involving hydrogen mobility on both the Pt and W_2C surfaces.

To optimize the p-Si/W_2C photocathodes, we performed PEC measurements on photocathodes with different W_2C thicknesses (25, 49, 99, and 148 Å) and annealing temperatures (as deposited, 350, 450, and 550 °C). The LSV scans for these films are included in the Supporting Information (Figures S3 and S4). The p-Si/W_2C photocathodes with W_2C thicknesses of 25 and 49 Å showed similar limiting photocurrent densities. As the thickness increased to 99 and 148 Å the limiting photocurrent density decreased, presumably due to increased reflection by the thicker films. p-Si/W_2C photocathodes with a W_2C thickness of 49 Å showed similar photocurrent onset potentials and photocurrent densities regardless of the annealing temperature (as deposited, 350, 450, and 550 °C). However, annealing in Ar improved the stability of the p-Si/W_2C photocathodes and resulted in higher photocurrents after depositing Pt nanoparticles. The photocathodes that were not annealed may have oxidized during the anodic segment of the current controlled pulsed deposition. Other researchers have reported that transition metal carbides can be passivated and stabilized for certain chemical reactions by annealing in oxygen following synthesis.[33,34] We chose an annealing temperature of 450 °C for further characterization because there appeared to be a loss of crystalline W_2C after annealing to temperatures of ≥550 °C as explained in the X-ray diffraction results later.

Electrochemical Results. Electrochemical measurements were performed on the FTO/W_2C electrodes to test their resistance to oxidation and assess W_2C as a support for Pt nanoparticles. Figure 4a shows a cyclic voltammetry (CV) scan for FTO/W_2C electrodes with a W_2C thickness of 148 Å as deposited and after annealing in Ar at 450 °C for 2 h. The initial scan direction was from negative to positive potentials (segment 1) followed by a scan in the opposite direction (segment 2). The FTO/W_2C electrode that was not annealed produced a peak in anodic current at potentials more positive

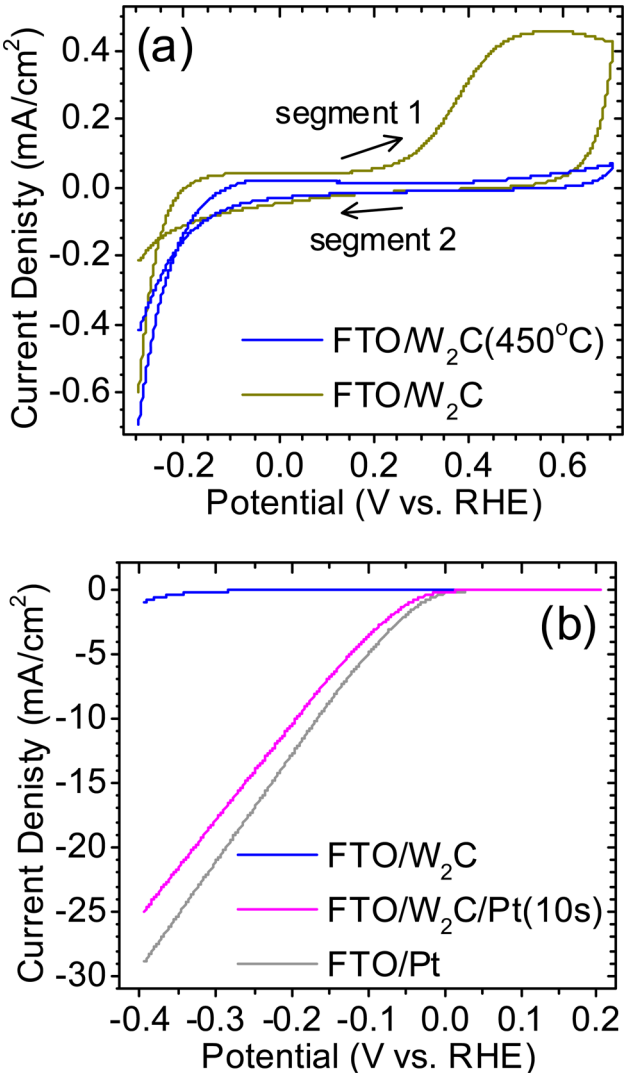

Figure 4. (a) CV scans of FTO/W_2C electrodes as deposited and annealed in Ar flow at 450 °C. The initial scan direction (segment 1) was from negative to positive potentials followed by a scan in the reverse direction (segment 2). (b) LSV scans of FTO/W_2C electrodes that were annealed at 450 °C in Ar with and without Pt nanoparticles deposited on the surface for 10 s along with an LSV scan of a dense Pt film on FTO. The FTO/W_2C electrodes had a W_2C thickness of 148 Å. Measurements were conducted in N_2 purged 1 N H_2SO_4 using a scan rate of 25 mV/s without *iR* compensation.

than 0.2 V vs RHE, which can be attributed to oxidation of the W_2C film. After CV testing the W_2C film was visibly transparent where it had been in contact with the electrolyte. In contrast, the FTO/W_2C electrode that was annealed did not produce significant anodic current during the CV scan or change noticeably in appearance. Weidemen et al., used chronopotentiometric (CP) titrations to create potential vs pH stability maps for WC, W_2C, and Mo_2C.[35] In acid environments (pH < 1), WC and W_2C did not undergo surface oxidation/dissolution as long as the potentials were more negative than 0.86 and 0.46 V vs RHE, respectively. The W_2C films deposited by RBD and annealed in Ar appear to be stable within a similar potential range in 1 N H_2SO_4. Figure 4b shows a LSV scan for annealed FTO/W_2C electrodes with and without Pt nanoparticles deposited on the surface for 10 s and the LSV scan for a dense Pt film on FTO. At potentials more

dx.doi.org/10.1021/ja411604k | J. Am. Chem. Soc. 2014, 136, 1535−1544

negative than 0.0 V vs RHE, the FTO/W_2C/Pt(10s) electrode behaved similar to the dense Pt film with the current density increasing at a much faster rate than for FTO/W_2C. A Tafel plot was constructed from LSV scans at a slower scan rate of 1 mV/s and is included in the Supporting Information (Figure S5). The plot shows that the FTO/W_2C/Pt/(10s) electrode and Pt film have nearly identical Tafel slopes and exchange current densities (log(Current Density) at 0 V vs RHE). This result is consistent with previous reports for Pt monolayers on W_2C (ML Pt–W_2C).[17]

X-ray Diffraction Results. The p-Si and p-Si/W_2C photocathodes were measured by XRD to determine the crystallinity of the W_2C films following synthesis by RBD and annealing in Ar. To obtain an adequate XRD count rate the W_2C films were deposited to a thickness of 148 Å. Figure 5

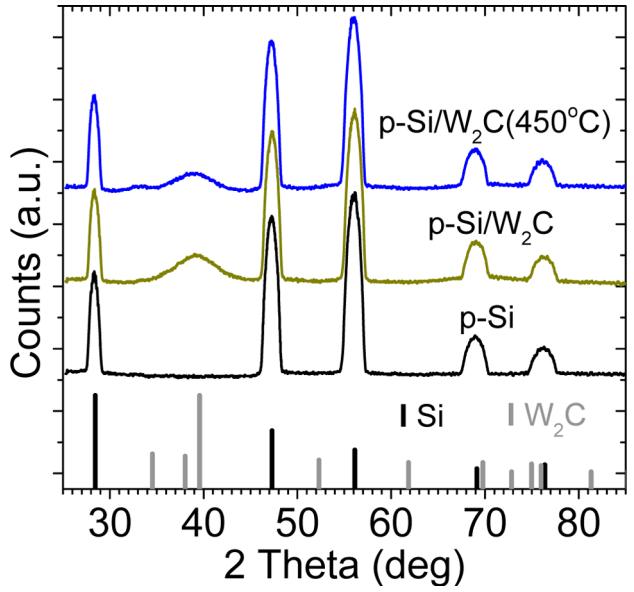

Figure 5. XRD spectra for p-Si and p-Si/W_2C as deposited and after annealing in Ar flow at 450 °C as indicated. The W_2C layer was 148 Å thick. The black vertical lines are the reference pattern for Si (PDF no. 00-027-1402) and the gray vertical lines are the reference pattern for W_2C (PDF no. 00-035-0776).

shows XRD spectra for p-Si and p-Si/W_2C photocathodes as deposited and after annealing in Ar at 450 °C for 2 h. The reference patterns for Si (PDF no. 00-027-1402) and W_2C (PDF no. 00-035-0776) are also included. The spectrum for bare p-Si(111) contained peaks for different lattice planes because the sample was rotated during the measurement. All peaks matched the reference pattern for Si. The p-Si/W_2C photocathode as deposited showed one additional peak besides the Si peaks. It was a broad peak at a two theta value of 39.6 deg, which matched the highest intensity line in the reference pattern for W_2C corresponding to the (101) plane. Thus, the W_2C films possessed some level of W_2C crystallinity even when deposited at ambient temperatures. After the p-Si/W_2C photocathode was annealed in Ar at 450 °C the main peak at 39.6 deg became smaller and another peak began to emerge at a 2 theta value of about 33 deg. Additional XRD spectra for p-Si/W_2C photocathodes annealed in Ar at various temperatures (as deposited, 350, 450, 550 °C) are displayed in Figure S6 in the Supporting Information. After the photocathode was annealed at 550 °C the peak at 33 deg became much more prominent and the W_2C(101) peak at 39.6 deg was nearly gone suggesting that the film no longer contained crystalline W_2C.

One advantage of synthesizing thin films by RBD is that crystalline materials can be deposited at relatively low substrate temperatures because the evaporated metal atoms are in a highly reactive state when they strike the surface of the substrate. RBD was previously used to grow crystalline MgO at −73 to 63 °C with Mg as the evaporant source in an ambient of oxygen (1×10^{-6} to 1×10^{-5} Torr).[20] Crystalline TiC was also deposited by RBD at 35 °C by evaporating Ti in a background of ethylene (~2×10^{-7} Torr).[22] In this work the p-Si(111) substrate temperature was not controlled during deposition although the e-beam evaporator provided some radiative heating. The temperature of the stainless steel substrate holder was measured to be about 50 °C during deposition. This is noteworthy because synthesis of transition metal carbides by thermal cracking in ethylene typically requires annealing temperatures above 600 K.[36] To fully carburize tungsten to WC, annealing temperatures above 1000 K are often needed.[37] Vapor phase synthesis techniques can be used to lower the formation temperature of W_2C and WC. With magnetron sputtering from a WC target, the substrate temperature, reactant gases, and postannealing conditions can be adjusted to control the W to C ratio.[8,17,38] At a substrate temperature of 400 °C, magnetron sputtering in pure Ar will result in W_2C, while leaking in hydrogen and ethylene (H_2:C_2H_4 ratio of 2:1) can produce WC.[17] Although we synthesized W_2C films using a single temperature, it may be possible to synthesize WC by evaporation of W in ethylene at slightly higher substrate temperatures.

X-ray Photoelectron Spectroscopy. The p-Si/W_2C photocathodes were measured using XPS to investigate the elemental composition. XPS spectra were obtained for the W 4f, C 1s, Si 2s, and O 1s binding energy regions. Ar sputtering was used to probe below the W_2C surface. Figure 6 shows XPS spectra for a p-Si/W_2C photocathode that had been annealed in Ar at 450 °C. The measurements were performed after Ar sputter times of 0, 1, and 10 s as indicated. Figure 6a shows that the W $4f_{5/2}$ and W $4f_{7/2}$ peaks were located at binding energies of 33.8 and 31.6 eV, respectively, which is 0.2 to 0.8 eV positive of the binding energies for W metal.[39] Ar sputtering increased the W 4f peak heights but did not shift their locations. Figure 6b shows the C 1s spectra and reveals that before Ar sputtering the W_2C films were covered with a layer of adventitious carbon since the C 1s peak was located at 284.3 eV. After 1 s of Ar sputtering the C 1s peak broadened due to overlap in signal from the adventitious carbon and the carbon bonded to tungsten in the W_2C film and after 10 s there was a single C 1s peak at 283.2 eV. This is the expected peak location for W_2C rather than WC, which typically shows a C 1s peak at a slightly lower binding energy.[17] Figure 6c shows the XPS spectra for the O 1s. Before Ar sputtering there was an O 1s peak centered a 530.5 eV with a small shoulder at higher binding energy. After 10 s of Ar sputtering the O 1s signal was diminished indicating that the W_2C films were mainly oxidized on the surface. We discovered that the W_2C surface oxidized readily even at relatively low partial pressures of oxygen and water. An additional p-Si/W_2C photocathode was measured by XPS after transferring from the high vacuum deposition chamber (5×10^{-8} Torr) into a vacuum tight capsule (estimated at $\leq 10^{-5}$ Torr) and then from the capsule into the XPS chamber. This photocathode still showed a significant O 1s signal at the surface.

dx.doi.org/10.1021/ja411604k | J. Am. Chem. Soc. 2014, 136, 1535–1544

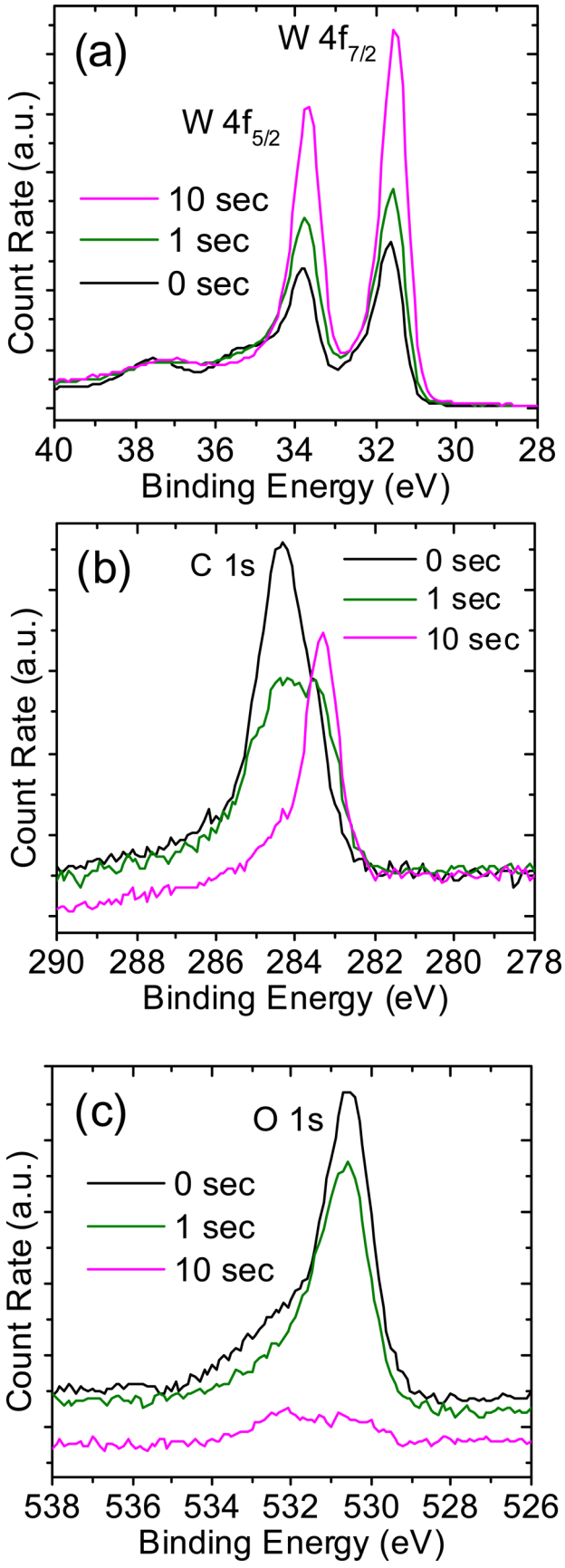

Figure 6. XPS spectra for (a) W 4f, (b) C 1s, and (c) O 1s regions after various Ar sputter times (0, 1, and 10 s) for a p-Si/W_2C photocathode that was annealed in Ar at 450 °C.

XPS was used to create concentration depth profiles for the p-Si/W_2C photocathodes and determine the bulk W:C atomic ratio below the surface. The atomic concentration of W, C, O, and Si were calculated by integrating the areas under the XPS spectra and subtracting the background using the Shirley method.[40] To distinguish between adventitious surface carbon and carbon in the W_2C films, the C 1s peaks located at 284–285 eV were not used in the calculations. Concentration depth profiles for p-Si/W_2C photocathodes as deposited and after annealing at 450 °C in Ar are shown in Figure S7 in the Supporting Information. The shapes of the concentration depth profiles were slightly different. The annealed p-Si/W_2C photocathode had a broader distribution of W and C, which trailed off after longer Ar sputtering times. This may have been due to a slower Ar sputtering rate for the annealed W_2C film. As shown in the electrochemical results above, the annealed W_2C film was more stable in electrolyte and less susceptible to damage by oxidation. Additionally, W and C may have diffused into the p-Si substrate during annealing. After 7 s of Ar sputtering the p-Si/W_2C photocathodes as deposited and annealed both showed W:C atomic ratios of approximately 1.8:1, which is close to the expected ratio of 2:1 for W_2C. Nevertheless, the films may contain a slight excess of carbon in addition to the crystalline W_2C that was revealed by XRD.

XPS was also performed on p-Si and p-Si/W_2C photocathodes with Pt nanoparticles on the surface. Figure 7 shows

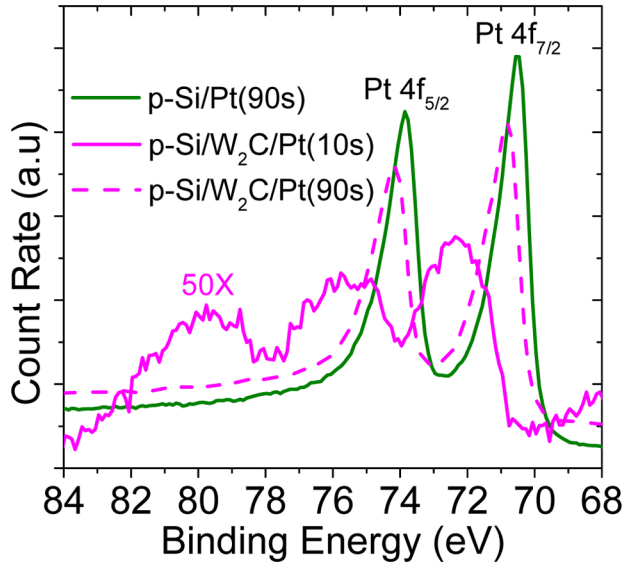

Figure 7. XPS spectra for the Pt 4f region for p-Si/(90s), p-Si/W_2C/Pt(10s), and p-Si/W_2C/Pt(90s) photocathodes after PEC testing and Pt deposition. The p-Si/W_2C/Pt photocathodes had a W_2C thickness of 49 Å and had been annealed in Ar at 450 °C. The count rate for p-Si/W_2C/Pt(10s) was multiplied by 50.

the Pt 4f region XPS spectra for p-Si/(90s), p-Si/W_2C/Pt(10s), and p-Si/W_2C/Pt(90s) photocathodes that had been used for PEC measurements. The p-Si/Pt and p-Si/W_2C/Pt(90s) photocathodes had Pt $4f_{5/2}$ and $4f_{7/2}$ peaks at binding energies of 73.9–74.1 and 70.5–70.8 eV, respectively, which is characteristic of Pt metal.[39] The p-Si/W_2C/Pt(10s) photocathode produced a much lower XPS count rate (signal multiplied by 50), which is reasonable considering that it contained perhaps 1/9 as much Pt and smaller Pt nanoparticles. It also showed a shift in the Pt 4f peak locations to higher

dx.doi.org/10.1021/ja411604k | J. Am. Chem. Soc. 2014, 136, 1535–1544

binding energies with two peaks at 75.7 and 72.4 eV and a third peak at 79.8 eV. This may have been due to surface oxidation of the Pt nanoparticles as well as an electronic interaction between the Pt nanoparticles and the W_2C film. As mentioned earlier, DFT calculations predicted a strong interfacial interaction between W and Pt d-states for Pt monolayers on WC.[27,28] The DFT calculations did not consider Pt f-states, but XPS produces a higher signal for the Pt 4f region compared to other Pt regions.

Time-of-Flight Secondary Ion Mass Spectrometry. Time of flight secondary ion mass spectrometry (TOF-SIMS) was employed to investigate the chemical composition of the W_2C films and the corresponding W_2C−Si interfaces. To attain a reasonable depth resolution while resolving the very thin W_2C layers, the depth profiles were acquired in a special SIMS dynamic profiling mode with a low current (~3 pA) primary ion beam (Bi_1^+ at 30 keV), which was used for both probing and sputtering.[41] Owing to edge sputtering effects all depth profiles were reconstructed from the initial raw data by using an identical region of interest centered within the primary ion beam raster area of 20 μm × 20 μm. All detected secondary ions had positive polarity and a mass resolution better than 3000 (m/δm). The sputtering rates of W_2C (~0.31 Å/s) and Si (~0.042 Å/s) were determined based on knowledge of the W_2C thickness and a previously sputtered Si wafer. An improved interfacial rate model was used to convert the sputtering time into depth.[42] The normalized secondary ion yields of W_2C^+ (marker for the W_2C film) and Si_2^+ (marker for the Si substrate) are shown in Figure 8a and 8b for p-Si/W_2C photocathodes as deposited and after annealing in Ar at 450 °C, respectively. The dynamic profile of the annealed p-Si/W_2C photocathode showed higher levels of contaminants (Na, K) and oxygen at the surface. AFM measurements indicated a W_2C surface corrugation of less than 3 Å for both photocathodes (see Figure S8 in the Supporting Information). The atomic intermixing between the W_2C overlayer and the Si substrate (calculated at 10% of the W_2C^+ and Si_2^+ signals and corrugation deconvoluted[42,43]) were ~6.7 and ~8.7 nm, as deposited and after annealing, respectively. Thus the annealing process induced the growth of a thin layer contamination, a thicker oxide at the W_2C surface, and additional atomic intermixing (2 nm) at the W_2C−Si interface. In addition, tungsten silicide (WSi_x) may have formed at the interface. Amorphous WSi_x films have been shown to undergo crystallization when annealed in Ar at 450 °C.[44] This may have contributed to the increased stability of the annealed p-Si/W_2C photocathodes during Pt deposition as well as improved charge transport at the W_2C−Si interface.

Transmission and Reflection Spectroscopy. Since W_2C is a reflective material, it is expected to reduce light transmission when deposited onto the surface of photocathodes as an electrocatalyst. To verify this, we used a UV−vis instrument with an integrating sphere to measure the transmission and reflectance of a p-Si photocathode and p-Si/W_2C photocathodes with 49 Å of W_2C on the surface (as deposited and after annealing in Ar at 450 °C). Figure 9a shows the transmission-reflectance (%T + %R) and transmission (%T) spectra for the photocathodes. %T + %R was obtained with the photocathodes inside the integrating sphere and %T was acquired with the photocathodes in front of the integrating sphere so the measurement does not distinguish between %R and light that is absorbed. Nevertheless, all of the spectra show a decrease in %T for light wavelengths less than 1150 nm

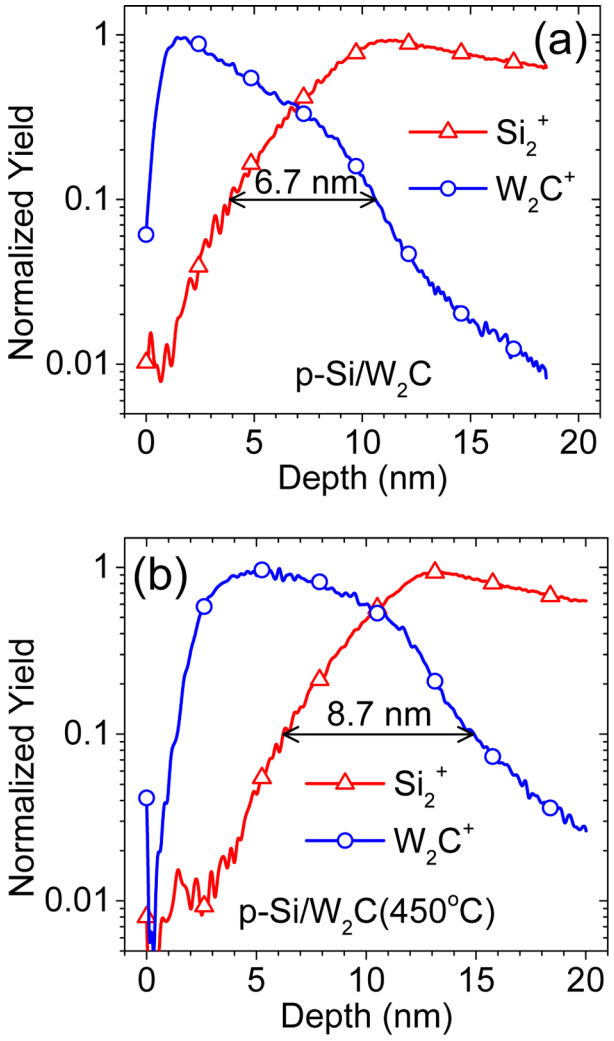

Figure 8. Dynamic depth profiles of W_2C^+ and Si_2^+ markers for p-Si/W_2C photocathodes (a) as deposited and (b) after annealing in Ar at 450 °C.

corresponding to light absorption by the p-Si substrate, which has an indirect bandgap of 1.12 eV.[2] %R can be estimated by subtracting the %T spectrum from the %T + %R spectrum for each photocathode (Figure 9b). The resulting %R spectra show that the p-Si/W_2C photocathodes reflect 20−30% more light than the bare p-Si photocathode for light wavelengths less than 1150 nm. We also measured %T for bare FTO and FTO/W_2C electrodes as deposited and after annealing (see Figure S10 in Supporting Information). The FTO/W_2C electrodes transmitted 20−40% less light than bare FTO at light wavelengths less than 1150 nm. So even while absorbing less light, the p-Si/W_2C photocathodes remain more photoactive for the HER than the p-Si photocathodes.

Photoelectrochemical Stability and Comparison with Ni−Mo. We checked the stability of annealed p-Si/W_2C and p-Si/W_2C/Pt(10s) photocathodes along with p-Si/Pt(90s) by performing long-term amperometric i−t scans (see Figure 10). The photocathodes were held at a constant potential of 0.005 V vs RHE under a white light intensity of 100 mW/cm^2 for 60 min. N_2 was bubbled through the cell and the surfaces of the photocathodes were continuously flushed with electrolyte using a peristaltic pump. The p-Si/W_2C and p-Si/W_2C/Pt(10s) photocathodes showed good stability over the course of 60 min

dx.doi.org/10.1021/ja411604k | J. Am. Chem. Soc. 2014, 136, 1535−1544

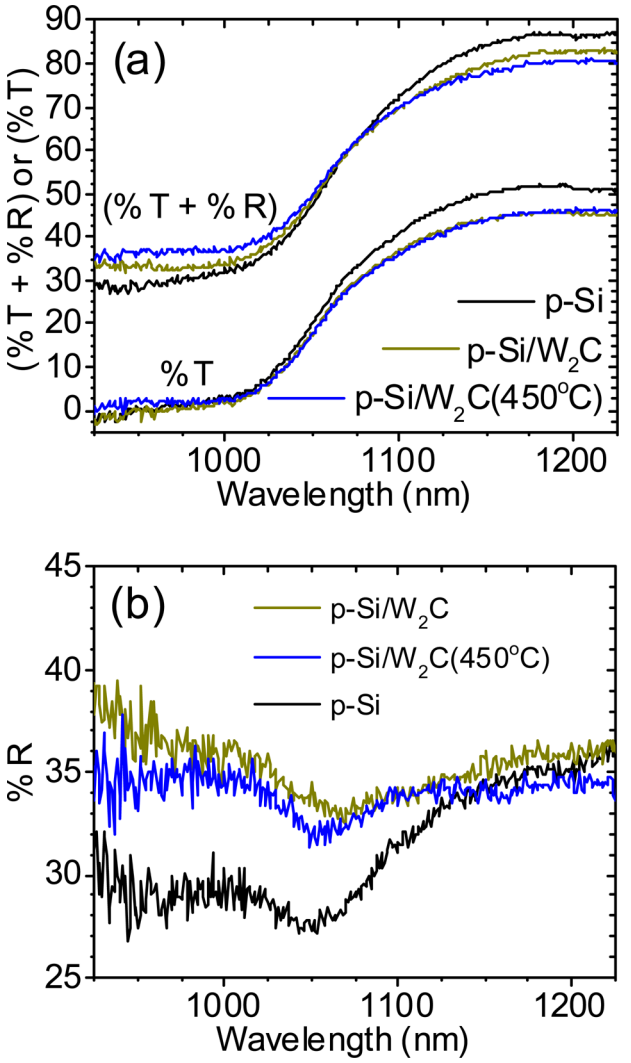

Figure 9. Transmission-reflectance spectra for p-Si and p-Si/W_2C photocathodes as deposited and annealed in Ar flow at 450 °C. The W_2C thickness was 49 Å. (a) Measured (%T + %R) and %T. (b) %R as calculated from the data in panel a.

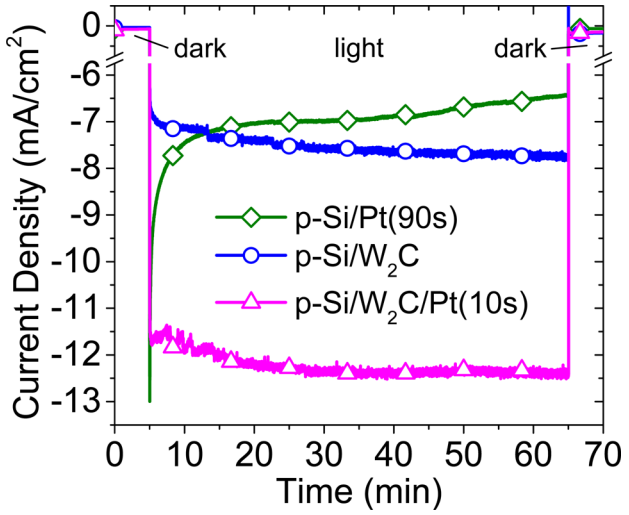

Figure 10. Amperometric i–t curve at a constant potential of 0.005 V vs RHE for a p-Si/Pt photocathode with 90 s of pulsed Pt deposition and p-Si/W_2C photocathodes with and without 10 s of pulsed Pt deposition. The p-Si/W_2C photocathodes were annealed under Ar flow at 450 °C and the W_2C thickness was 49 Å. Measurements were conducted in N_2 purged 1 N H_2SO_4 with the film surface continuously flushed using a peristaltic pump and a white light intensity of 100 mW/cm^2.

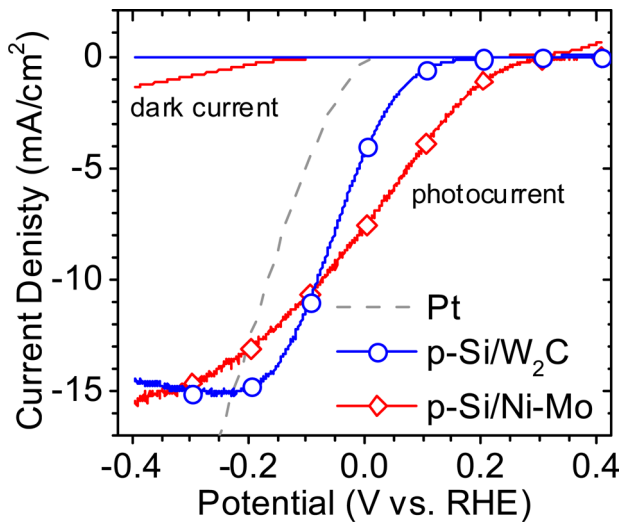

Figure 11. LSV scans (dark and white light) for p-Si/Ni–Mo and p-Si/W_2C photocathodes and a dense Pt film. The Ni–Mo and W_2C thicknesses were both estimated to be 49 Å. The p-Si/W_2C photocathodes were annealed under Ar flow at 450 °C. Measurements were conducted in N_2 purged 1 N H_2SO_4 with a scan rate of 25 mV/s and white light intensity of 100 mW/cm^2.

with the photocurrent density increasing slightly. The increase may have been the result of oxygen production by OER at the Pt counter electrode, which diffused to the photocathodes faster than it could be purged by N_2. The p-Si/Pt(90s) photocathodes did not produce photocurrent densities that were repeatable and stable over 60 min as demonstrated by the decay in photocurrent for p-Si/Pt(90s) in Figure 10.

Lastly, we compared the PEC performance of W_2C to Ni–Mo, another earth abundant material that has been studied as an electrocatalyst for HER on electrodes and Si-based photocathodes.[45−48] We tested four different Ni:M atomic ratios (7:1, 3:1, 1:1, and 3:5) and found that p-Si/Ni–Mo photocathodes with a Ni:M atomic ratio of 1:1 resulted in the highest photocurrent densities. A Ni:M atomic ratio of 1:1 has been suggested as the most catalytic atomic ratio for the HER.[49] Figure 11 shows the LSV scans for the p-Si/W_2C and p-Si/Ni–Mo photocathodes with equivalent W_2C and Ni–Mo film thicknesses of 49 Å. The p-Si/W_2C photocathodes were annealed in Ar at 450 °C but the p-Si/Ni–Mo photocathodes were not. The p-Si/Ni–Mo photocathodes showed a photocurrent onset potential of about 0.3 V vs RHE, which was slightly more positive than the p-Si/W_2C photocathode and more positive than that previously reported for the electrodeposition of Ni–Mo onto p-Si.[47] However, the p-Si/Ni–Mo photocathodes produced considerable anodic current at more positive potentials, and the photocurrent decreased with repeated testing so they were not stable. Ni–Mo has been reported to be stable in alkaline solutions for long periods of time but stability and passiviation requirements for Ni–Mo in acidic solutions are less substantiated.[50] We attempted to passivate the p-Si/Ni–Mo photocathodes by annealing in Ar flow at 450 °C for 2 h but it only worsened the photocurrent density. In summary, the p-Si/W_2C photocathodes demon-

dx.doi.org/10.1021/ja411604k | J. Am. Chem. Soc. 2014, 136, 1535−1544

strated a comparable photocurrent density to p-Si/Ni−Mo at 0.0 V vs RHE and better stability in acidic solution making W_2C another earth abundant option to use as an electrocatalyst material for solar hydrogen production.

CONCLUSIONS

We have synthesized p-Si/W_2C photocathodes by reactive ballistic deposition (RBD) and reported the photoelectrochemical (PEC) activity for the HER. X-ray diffraction (XRD) revealed that the W_2C films contained crystalline W_2C when deposited at ambient temperatures while X-ray photoemission spectroscopy (XPS) indicated a W:C atomic ratio close to 2:1. The W_2C film surface was passivated by annealing in Ar flow at 450 °C for 2 h, which improved stability in 1 N sulfuric acid. p-Si/W_2C photocathodes demonstrated cathodic photocurrent onset potentials more positive than 0 V vs RHE while the p-Si photocathode did not. The W_2C film was an effective support for Pt nanoparticles deposited by current controlled pulsed deposition allowing for a factor of 9 reduction in Pt loading. p-Si/W_2C photocathodes with Pt nanoparticles showed comparable photocurrent onset potentials and limiting photocurrent densities and better stability than p-Si photocathodes with 9 times as much Pt.

ASSOCIATED CONTENT

Supporting Information

Current controlled pulse deposition example, LSV scans, XRD spectra, UV−vis spectra, Tafel plot, and AFM data. This material is available free of charge via the Internet at http://pubs.acs.org.

AUTHOR INFORMATION

Corresponding Author

mullins@che.utexas.edu

Notes

The authors declare no competing financial interest.

ACKNOWLEDGMENTS

The authors gratefully acknowledge the Division of Chemical Sciences, Geosciences, and Biosciences, Office of Basic Energy Sciences of the U.S. Department of Energy through Grant DE-FG02-09ER16119, and the Welch Foundation (Grant F-1436) for funding this work. S.P. Berglund thanks the National Science Foundation Graduate Research Fellowship Program for financial support. The National Science Foundation funded the X-ray photoelectron spectrometer (Grant No. 0618242), and the TOF-SIMS instrument (ION-TOF GmbH, Germany, 2010) was purchased through the National Science Foundation Major Research Instrumentation program (DMR-0923096). We thank C.J. Stolle and B.A. Korgel for use of the Cary 500 spectrophotometer, and J.M. McCrate, T. D.-M. Elko-Hansen, and J.G. Ekerdt for assistance in cleaning and etching silicon (University of Texas at Austin).

REFERENCES

(1) Bard, A. J.; Fox, M. A. *Acc. Chem. Res.* **1995**, *28*, 141−145.
(2) Walter, M. G.; Warren, E. L.; McKone, J. R.; Boettcher, S. W.; Mi, Q.; Santori, E. A.; Lewis, N. S. *Chem. Rev.* **2010**, *110*, 6446−6473.
(3) Nakato, Y.; Tonomura, S.; Tsubomura, H. *Ber. Bunsen. Phys. Chem.* **1976**, *80*, 1289−1293.
(4) Dominey, R. N.; Lewis, N. S.; Bruce, J. A.; Bookbinder, D. C.; Wrighton, M. S. *J. Am. Chem. Soc.* **1982**, *104*, 467−482.
(5) Nakato, Y.; Yano, H.; Nishiura, S.; Ueda, T.; Tsubomura, H. *J. Electroanal. Chem. Interfacial Electrochem.* **1987**, *228*, 97−108.
(6) Yang, C.-J. *Energy Policy* **2009**, *37*, 1805−1808.
(7) Levy, R. B.; Boudart, M. *Science* **1973**, *181*, 547−549.
(8) Hwu, H. H.; Chen, J. G. *Chem. Rev.* **2004**, *105*, 185−212.
(9) Sokolsky, D. V.; Palanker, V. S.; Baybatyrov, E. N. *Electrochim. Acta* **1975**, *20*, 71−77.
(10) Armstrong, R. D.; Bell, M. F. *Electrochim. Acta* **1978**, *23*, 1111−1115.
(11) Nikolov, I.; Petrov, K.; Vitanov, T.; Guschev, A. *Int. J. Hydrogen Energy* **1983**, *8*, 437−440.
(12) Harnisch, F.; Sievers, G.; Schröder, U. *Appl. Catal. B: Environ.* **2009**, *89*, 455−458.
(13) Chen, W.-F.; Muckerman, J. T.; Fujita, E. *Chem. Commun.* **2013**, *49*, 8896−8909.
(14) Ma, C.; Sheng, J.; Brandon, N.; Zhang, C.; Li, G. *Int. J. Hydrogen Energy* **2007**, *32*, 2824−2829.
(15) Ham, D. J.; Ganesan, R.; Lee, J. S. *Int. J. Hydrogen Energy* **2008**, *33*, 6865−6872.
(16) Wu, M.; Shen, P. K.; Wei, Z.; Song, S.; Nie, M. *J. Power Sources* **2007**, *166*, 310−316.
(17) Esposito, D. V.; Hunt, S. T.; Kimmel, Y. C.; Chen, J. G. *J. Am. Chem. Soc.* **2012**, *134*, 3025−3033.
(18) Garcia-Esparza, A. T.; Cha, D.; Ou, Y.; Kubota, J.; Domen, K.; Takanabe, K. *ChemSusChem* **2013**, *6*, 168−181.
(19) Jang, J. S.; Ham, D. J.; Lakshminarasimhan, N.; Choi, W. y.; Lee, J. S. *Appl. Catal. A: Gen.* **2008**, *346*, 149−154.
(20) Dohnálek, Z.; Kimmel, G. A.; McCready, D. E.; Young, J. S.; Dohnálková, A.; Smith, R. S.; Kay, B. D. *J. Phys. Chem. B* **2002**, *106*, 3526−3529.
(21) Flaherty, D. W.; Dohnálek, Z.; Dohnálková, A.; Arey, B. W.; McCready, D. E.; Ponnusamy, N.; Mullins, C. B.; Kay, B. D. *J. Phys. Chem. C* **2007**, *111*, 4765−4773.
(22) Flaherty, D. W.; May, R. A.; Berglund, S. P.; Stevenson, K. J.; Mullins, C. B. *Chem. Mater.* **2009**, *22*, 319−329.
(23) Berglund, S. P.; Flaherty, D. W.; Hahn, N. T.; Bard, A. J.; Mullins, C. B. *J. Phys. Chem. C* **2010**, *115*, 3794−3802.
(24) Flaherty, D. W.; Hahn, N. T.; May, R. A.; Berglund, S. P.; Lin, Y.-M.; Stevenson, K. J.; Dohnalek, Z.; Kay, B. D.; Mullins, C. B. *Acc. Chem. Res.* **2012**, *45*, 434−443.
(25) Berglund, S. P.; Rettie, A. J. E.; Hoang, S.; Mullins, C. B. *Phys. Chem. Chem. Phys.* **2012**, *14*, 7065−7075.
(26) He, H.; Xiao, P.; Zhou, M.; Zhang, Y.; Jia, Y.; Yu, S. *Catal. Commun.* **2011**, *16*, 140−143.
(27) Ma, C. a.; Liu, T.; Chen, L. *Appl. Surf. Sci.* **2010**, *256*, 7400−7405.
(28) Vasić, D. D.; Pašti, I. A.; Mentus, S. V. *Int. J. Hydrogen Energy* **2013**, *38*, 5009−5018.
(29) Benson, J. E.; Kohn, H. W.; Boudart, M. *J. Catal.* **1966**, *5*, 307−313.
(30) Tseung, A. C. C.; Chen, K. Y. *Catal. Today* **1997**, *38*, 439−443.
(31) Prins, R. *Chem. Rev.* **2012**, *112*, 2714−2738.
(32) Esposito, D. V.; Levin, I.; Moffat, T. P.; Talin, A. A. *Nat. Mater.* **2013**, *12*, 562−568.
(33) Santos, J. B. O.; Valença, G. P.; Rodrigues, J. A. J. *J. Catal.* **2002**, *210*, 1−6.
(34) Patt, J.; Moon, D.; Phillips, C.; Thompson, L. *Catal. Lett.* **2000**, *65*, 193−195.
(35) Weidman, M. C.; Esposito, D. V.; Hsu, Y.-C.; Chen, J. G. *J. Power Sources* **2012**, *202*, 11−17.
(36) Chen, J. G. *Chem. Rev.* **1996**, *96*, 1477−1498.
(37) Benziger, J. B.; Ko, E. I.; Madix, R. J. *J. Catal.* **1978**, *54*, 414−425.
(38) Zellner, M. B.; Chen, J. G. *Catal. Today* **2005**, *99*, 299−307.
(39) Wagner, C. D.; Naumkin, A. V.; Kraut-Vass, A.; Allison, J. W.; Powell, C. J.; John, R. Rumble, J.; *NIST X-ray Photoelectron Spectroscopy Database*; National Institute of Standards and Technology: Gaithersburg, MD, August 15, 2007.
(40) Shirley, D. A. *Phys. Rev. B* **1972**, *5*, 4709.

(41) Nayak, A. P.; Dolocan, A.; Lee, J.; Chang, H.-Y.; Pandhi, T.; Tao, L. I.; Holt, M.; Akinwande, D. *Nano* **2013**, *0*, 1450002.
(42) Zimmerman, J. D.; Lassiter, B. E.; Xiao, X.; Sun, K.; Dolocan, A.; Gearba, R.; Vanden Bout, D. A.; Stevenson, K. J.; Wickramasinghe, P.; Thompson, M. E.; Forrest, S. R. *ACS Nano* **2013**, *7*, 9268−9275.
(43) Hofmann, S. *Thin Solid Films* **2001**, *398*−*399*, 336−342.
(44) Tsai, M. Y.; d'Heurle, F. M.; Johnson, R. W. *J. Appl. Phys.* **1981**, *52*, 5350−5355.
(45) Raj, I. A. *J. Mater. Sci.* **1993**, *28*, 4375−4382.
(46) Fan, C. L.; Piron, D. L.; Sleb, A.; Paradis, P. *J. Electrochem. Soc.* **1994**, *141*, 382−387.
(47) McKone, J. R.; Warren, E. L.; Bierman, M. J.; Boettcher, S. W.; Brunschwig, B. S.; Lewis, N. S.; Gray, H. B. *Energy Environ. Sci.* **2011**, *4*, 3573−3583.
(48) Lin, Y.; Battaglia, C.; Boccard, M.; Hettick, M.; Yu, Z.; Ballif, C.; Ager, J. W.; Javey, A. *Nano Lett.* **2013**, *13*, 5615−5618.
(49) Jakšić, J. M.; Vojnović, M. V.; Krstajić, N. V. *Electrochim. Acta* **2000**, *45*, 4151−4158.
(50) Brown, D. E.; Mahmood, M. N.; Man, M. C. M.; Turner, A. K. *Electrochim. Acta* **1984**, *29*, 1551−1556.